ELSEVIER

Coordination Chemistry Reviews
200–202 (2000) 1009–1032

COORDINATION CHEMISTRY REVIEWS

www.elsevier.com/locate/ccr

Spectroscopic identification of gas phase photofragments from coordination compound chemical vapor deposition precursors

Jinwoo Cheon [a,*], Hong-Kyu Kang [a], Jeffrey I. Zink [b,1]

[a] *Center for Molecular Science and Department of Chemistry, Korea Advanced Institute of Science and Technology (KAIST), Taejon 305-701, South Korea*
[b] *Department of Chemistry and Biochemistry, University of California, Los Angeles, CA 90095, USA*

Received 14 October 1999; accepted 24 February 2000

Contents

* Corresponding author.
[1] Also corresponding author. Tel.: +1-310-8251001; fax: +1-310-2069880.
E-mail address: zink@chem.ucla.edu (J.I. Zink).

PII: S0010-8545(00)00325-8

Abstract

This review focuses on the gas phase photochemical fragmentation processes of coordination compounds that are precursors for the laser driven synthesis of solid-state materials such as thin films and nanoclusters from the gas phase. Specific emphasis is placed on the identification of photofragments by luminescence spectroscopy during the deposition process. In several cases, results from mass spectroscopy and from photofragmentation under the collision-free conditions of a molecular beam are included to clarify the identifications and mechanisms. Detailed experimental measurements have been made on metal diketonates, metal amides, metal xanthates and metal thiocarbamates. These compounds are useful as molecular precursors for the synthesis of thin films and nanoparticles of metals, binary and ternary materials, and semiconductor films.

Keywords: Semiconductor; Photofragments; Metal diketonates

1. Introduction

Coordination compounds are important precursors for solid-state materials synthesis [1]. Volatile coordination compounds are especially important as precursors for thin films or nanocluster synthesis by chemical vapor deposition (CVD). CVD is a process where a precursor molecule is decomposed to deposit a desired thin film material. Thermal (pyrolytic) CVD chemistry of coordination compounds is the most widely studied, but investigations of laser-assisted CVD (LCVD) using coordination compound precursors is attracting increasing interest. LCVD processes have the advantages of spatial selectivity of deposition on the substrate, selective energy transfer to the deposition precursor, and low processing tempera-

tures [2]. Efforts to fabricate multi-layer structures with well-defined physical properties and abrupt interfaces benefit from the low growth temperatures. With this technique, patterned features of the desired materials can be drawn in 'real time' in a one- or two-step process compared with the many steps involved with lithographic techniques.

Recent reports indicate that under LCVD conditions luminescence is often observed, and luminescence spectroscopy can then identify photofragments in the gas phase and assist in the elucidation of the photolytic deposition pathways [4–10]. The effects of changing the deposition conditions can be determined by observing the corresponding changes in the spectra. In addition, luminescence spectroscopy can determine product internal energies and relaxation that are important to explain the laser deposition process. 'Real time' chemical information about activated gas phase species involved in materials growth on substrates is difficult to obtain but is very important for better understanding and improving the CVD process.

Gas phase photochemistry is substantially different from photochemistry in condensed media. The photoreactions can be initiated by excitation of the coordination compounds into ligand field and charge transfer excited states, as in the solution phase, but absorption of an additional photon or photons ('multiphoton absorption') is common because of less efficient relaxation pathways [3]. Multiphoton absorption populates highly energetic excited states which leads not only to dissociation of ligands from metal centers, but also to ligand fragmentation. Sequential absorption of photons by photoproducts (secondary photototolysis) is also common in the gas phase. In general, understanding of the photoactivated decomposition and identifying the photofragments is very important to the overall understanding and control of the composition and morphology of the desired solid-state product.

The focus of this review is on the spectroscopic identification of photofragments that are produced in the gas phase under the same conditions as those used for LCVD [4–10]. In several cases, results from mass spectroscopy and from photofragmentation under the collision-free conditions of a molecular beam are included to clarify identifications and mechanisms. The scope of this review encompasses research from the authors' laboratories on metal diketonates, metal amides, metal xanthates, and metal thiocarbamates.

The review is organized into three parts. First, metal hexafluoroacetylacetonate complexes are reviewed. For these complexes, usually an undesirable photofragment containing both the metal and a fluorine or carbon is found as a result of the photolysis. Details of the spectroscopy and mechanisms that were proposed for the reaction are discussed. Second, zinc and cadmium xanthate and thiocarbamate complexes are reviewed. The photochemical reactions that produce solid metal sulfide semiconductor films are discussed. Identification of photofragments in the gas phase is reviewed. Finally amide complexes of titanium, zirconium and hafnium that lead to the formation of metal nitride films are reviewed. LCVD of TiN, and gas phase identification of the desired metal nitrides are discussed.

2. Luminescence spectroscopic identification of photofragments from metal hfac compounds

The goal of LCVD is to use light to fragment the precursor molecules and deposit a desired product such as a pure metal. The large precursors that might emit light are photofragemented under the high laser fluence and extensive fragmentation occurs. When the fragments luminesce, spectroscopic analysis can be used to identify them.

Metal acetylacetonate (2,4-pentanedionate = acac) complexes have found utility as CVD precursors [11–13] including applications in metallization for semiconductor interconnects [14] and preparation of metal oxides for high Tc superconducting films [15]. Fluorinated acetylacetonate ligands (1,1,1,5,5,5-hexafluoro-2,4-pentanedionate = hfac) increase sample volatility and allow for more facile transport in the gas phase but may result in fluorine contamination of the final deposit [16]. For example, photolytic CVD of copper from $Cu(hfac)_2$ shows measurable fluorine incorporation [17,18].

In this section of the review, the luminescence that is observed under gas phase photolytic deposition conditions is discussed for Cu, Cr, Ni, and Pt hfac compounds. This luminescence is analyzed under a variety of conditions including the relatively wide range of pressures available in an evacuated gas cell, and under the collision free conditions of a molecular beam. Features in these spectra indicate that, in general, multiple photolysis processes occur. Simple fragments that are produced from these compounds are identified and the differences and similarities between the compounds are discussed. Detailed analysis of the spectra allows characterization of the internal energies of the fragments to be determined.

2.1. $Cu(hfac)_2$ [9]

The emission spectrum from $Cu(hfac)_2$ excited at 308 nm at 'high' pressure (sample + argon $= \sim 1$ bar) is shown in Fig. 1a. There are sharp peaks at 493.0, 510.5, 515.0, 521.8, 578.2 and 589.2 nm, and a broad feature with irregular but reproducible structure at 468.6 nm.

Under 308 nm excitation and low pressure conditions (sample pressure less than or equal to its vapor pressure) the spectrum in Fig. 1b is observed. There are no sharp lines between 310 and 425 nm, but there are peaks at 426.7, 437.9, 449.5, 461.7, 473.6, 476.8, 491.7, 505.1, 519.3, 545.6, 564.7, 567.6, 579.3 and 681.0 nm. The peaks at 491.7, 505.1 567.6 and 681.0 nm have a poorly resolved but regular structure. Similar results are observed for excitation at 360 nm.

Under the collision free conditions of the molecular beam and 308 nm excitation the spectral features present under the low pressure conditions resolve into distinct structured bands (Fig. 2). Molecular beam fluorescence excitation spectra taken in the range of 350–370 nm show no sharp features, but the dispersed fluorescence is the same as that observed with 308 nm excitation. The features at 449.5, 491.7, 505.1 and 567.6 nm, display quadratic power dependencies in the molecular beam as shown in the inserts of Fig. 2.

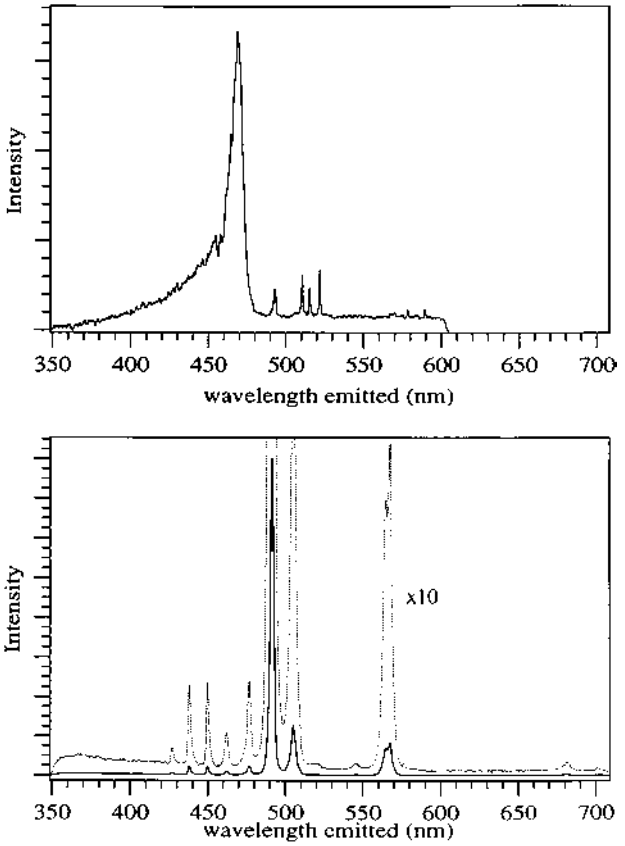

Fig. 1. Emission spectra observed from 308 nm excitation of $Cu(hfac)_2$ in the gas phase. Top: spectrum observed using a static chamber at a pressure of 1 bar; bottom: spectrum observed at a pressure no greater than the vapor pressure of $Cu(hfac)_2$.

2.1.1. Copper atom and cluster emission

The sharp lines in the high pressure 308 nm excited luminescence spectra are the Cu atomic transitions $4s^2\ ^2D \rightarrow 4p^2\ ^2P^0$ at 510.5 nm, $4p^2\ ^2P^0 \rightarrow 4d^2\ ^2D$ at 515.0 nm, $4p^2\ ^2P^0 \rightarrow 4d^2\ ^2D$ at 521.8 nm, and $4s^2\ ^2D \rightarrow 4p^2\ ^2P^0$ at 578.2 nm [14]. The broad feature at 468.6 nm includes contributions from Cu_2. Production of luminescent copper atoms from laser excitation of copper complexes is well known [19,20]. Three 193 nm photons are required to produce bare fluorescent Cu from $Cu(hfac)_2$ but two 193 nm photons (103 600 cm^{-1}) are insufficient to produce the bare metal. Thus, even three 308 nm photons would be insufficient to produce bare metal from the complex in the gas phase. In contrast, the threshold for bare metal atom production from the nonfluorinated complex is two 308.6 nm photons or 8.03 eV using multiphoton dissociation/ionization (MPD/MPI) [21]. Direct loss of both of the acetylacetonate ligands results from the coherent two UV photon excitation of a superexcited state at 8.03 eV.

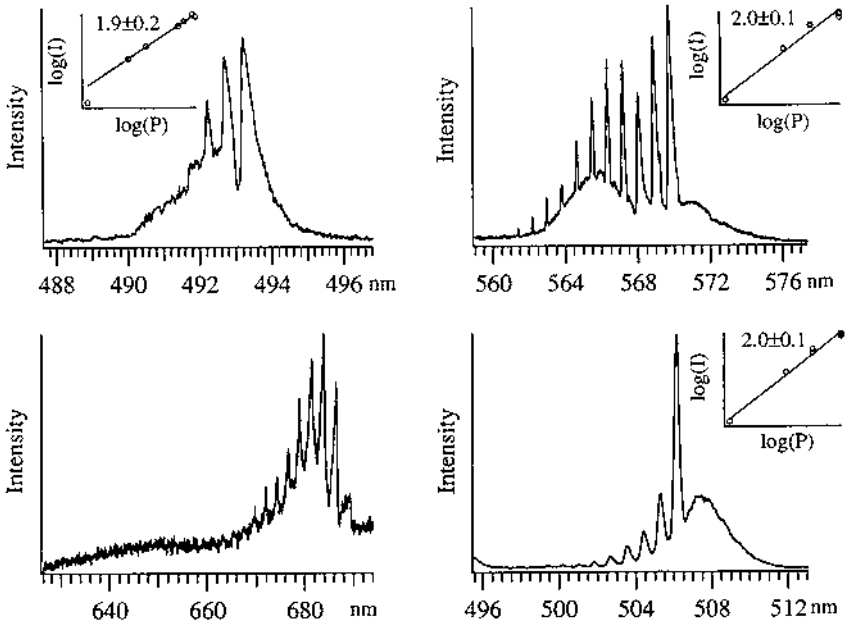

Fig. 2. Emission spectra of CuF arising from 308 nm excitation of $Cu(hfac)_2$ in a molecular beam. The inserts in each panel show the laser power dependence of the spectrum shown in that panel.

2.1.2. CuF emission

All of the 308 nm excited features in the low pressure chamber and the molecular beam were assigned to CuF luminescence. Excitation at 361 nm also results exclusively in CuF luminescence under low pressure conditions and in the molecular beam. CuF is ejected from $Cu(hfac)_2$ in an electronically excited state and is not resonantly excited by the laser.

The laser power dependence of the intensity of the CuF bands at 449.5, 491.7, 505.1 and 567.6 nm is quadratic. Two 308 nm photons have enough energy (64914 cm^{-1}) to break all four metal–oxygen bonds. Because a high fluence excitation source (~ 2 MW cm^{-2}) was used, however, transitions could be saturated so this luminescence should be viewed as being a result of at least two 308 nm photons. Saturation effects may, in general, complicate the interpretation of experimentally derived power laws.

The comparisons between the low and high pressure studies of $Cu(hfac)_2$ show that there are multiple pathways for photofragmentation of this complex. When collisions are present bare metal atoms and metal dimers are produced in an excited state. These channels do not appear in low collision and collision free conditions implying that the production of bare metal at 308 nm is not a strictly unimolecular photodissociation reaction.

The formation of CuF is endoergic with respect to the formation of Cu for ground state $Cu(hfac)_2$. Interestingly, under collision-free conditions only lumines-

cence from CuF is observed. The cleavage of the four metal–oxygen bonds requires 157 kcal mol^{-1} [22] of the 185.5 kcal mol^{-1} available from two 308 nm photons, leaving just enough energy (28 kcal mol^{-1}) to cleave the C–F bond and form the CuF bond. However, the CuF fragment has up to 66.4 kcal mol^{-1} of electronic excitation. There are two possible explanations for this discrepancy. The first is that the ligand fragments combine or rearrange to provide the required energy. The second, and simpler, explanation is that a third photon is exciting a saturated transition, giving an apparent quadratic power law.

Boltzmann fits to the spectra from the molecular beam studies show that the ejected CuF is both rotationally and vibrationally hot. The observed temperatures are on the order of 1700 K. The amount of energy disposed of in electronic and vibrational excitation is approximately 27 000 cm^{-1}. Nonstatistical vibrational populations are observed and can be explained in part by internal conversion of electronic excitation to vibrational excitation.

2.2. Ni(hfac)$_2$ [10]

Under 308 nm excitation and low pressure conditions (pressure less than or equal to the vapor pressure of the compound), the spectrum contains a multitude of sharp peaks between 340 and 550 nm. Under the collision free conditions of the molecular beam and 308 nm excitation the spectral features present under the low pressure conditions resolve into distinct structured bands [9].

2.2.1. Luminescence from nickel atoms

The intense sharp lines observed in both the gas cell spectrum and the molecular beam are assigned to nickel atomic lines. The majority of the new bands appearing in the molecular beam spectra are also attributable to Ni atomic lines. Nickel atomic lines are observed under all conditions studied. The observation of nickel atomic lines under CVD conditions is not unexpected for Ni(hfac)$_2$. Their observation, however, does confirm that nickel atoms are produced in the gas phase due to laser photolysis.

2.2.2. Luminescence from nickel fluoride

A number of bands were assigned to NiF emission based on comparison with known emission bands in the literature. The bands due to NiF do not have well resolved rotational band profiles beyond one case of a doubled band head at 451.6 nm. Nevertheless, the observation of these states of NiF clearly demonstrates the presence of NiF and shows that metal fluoride production is not unique to copper in the photofragmentation of metal hfac compounds.

2.3. Cr(hfac)$_3$ [10]

The spectra obtained from the low pressure gas cell from the chromium compound are substantially richer in features than those from the nickel compound. In the red and near infrared region of the emission spectrum a broad vibronic feature

is observed that is centered at approximately 13 000 cm^{-1} and is highly structured. The peaks are clustered into well-defined groups. The spacing between each group of peaks is approximately 585 cm^{-1}, while the spacing between individual adjacent peaks ranges from 85 to 125 cm^{-1}. There are at least five well-defined groupings of peaks. This band system extends from 15 500 to 10 000 cm^{-1}. In the visible region of the spectrum (25 000–16 000 cm^{-1}) many intense sharp (fwhm = 10 cm^{-1}) line features are observed. In addition there are many broader features observed at 23 154, 22 498 and 21 814 cm^{-1}. At energies higher than the 308 nm laser excitation source a long regular vibronic progression centered at 37 000 cm^{-1} is observed. The band consists of eight vibronic features but is obscured to lower energy by the presence of the laser line. The spacing between features is approximately 650 cm^{-1}. The bands have an average fwhm of approximately 300 cm^{-1}. Features are observed between 35 000 and 40 000 cm^{-1}.

All of the features discussed above are also observed in the molecular beam, but many new features appear. The assignments are discussed below.

2.3.1. Luminescence from chromium atoms

The intense sharp lines observed in both the gas cell spectrum and the molecular beam are assigned to atomic chromium emission. Chromium atomic lines are observed under all conditions studied. Their observation confirms that chromium atoms are produced in the gas phase due to laser photolysis.

2.3.2. Luminescence from chromium fluoride

The highly structured luminescence observed in the high pressure gas cell centered at 850 nm under 343 nm excitations is assigned as the transition from the $A^6\Sigma$ excited state of CrF to the $X^6\Sigma$ ground state. The $B^6\Sigma$ state of CrF is at 16 864 cm^{-1} and may be contributing to the spectral congestion in this region. The molecular beam produces molecules which are colder initially and which would be expected to have slower rates of internal conversion. In addition the lack of collisions prevents relaxation to the lowest excited state($A^6\Sigma$) of CrF. These factors all contribute to the molecular beam spectra being far richer in features and correspondingly more congested.

The $B^6\Sigma \rightarrow X^6\Sigma$ luminescence from CrF is clearly observed in the molecular beam spectrum. Bands observed in the blue region of the spectrum have a spacing characteristic of CrF. No electronic state for CrF in this region has been previously reported, however the characteristic spacing is a strong indication that this a previously unknown state of CrF.

2.4. $Pt(hfac)_2$ [10]

Fig. 3 displays the luminescence spectra obtained from $Pt(hfac)_2$ in the low pressure gas cell. The spectrum consists of many features, all of which are observed under both 308 and 440 nm excitation.

Under 440 nm excitation and low pressure conditions (cell pressure less than or equal to the vapor pressure of the compound), the spectrum in Fig. 3A is observed.

In the visible region a well-defined vibronic progression is observed. This band system has its origin at approximately 18 500 cm^{-1}. To higher energy from the origin there are many peaks in the region from 445 to 530 nm with prominent peaks at 517, 497, and 477 nm.

Under 'high' pressure conditions with added Ar buffer gas to a total pressure of ~ 1 bar, similar spectra are observed as illustrated in Fig. 3B. However, the peaks to high energy show reduced intensity as is apparent by comparing Fig. 3A and B. In particular the bands between 445 and 530 nm show different relative intensities. Also, the smaller peaks in the main progression to lower energy show reduced intensity.

2.4.1. Luminescence from platinum carbide

All major luminescence features present in Fig. 3 can be assigned to the $A \rightarrow X$ transition of PtC. There are no features present which can be assigned to either Pt atoms or PtF. It is possible that Pt atoms may be present in nonluminescent states. Spectral congestion in the hot band region from 445 to 530 nm may be obscuring some small features, however, all clearly identifiable peaks are assignable to PtC.

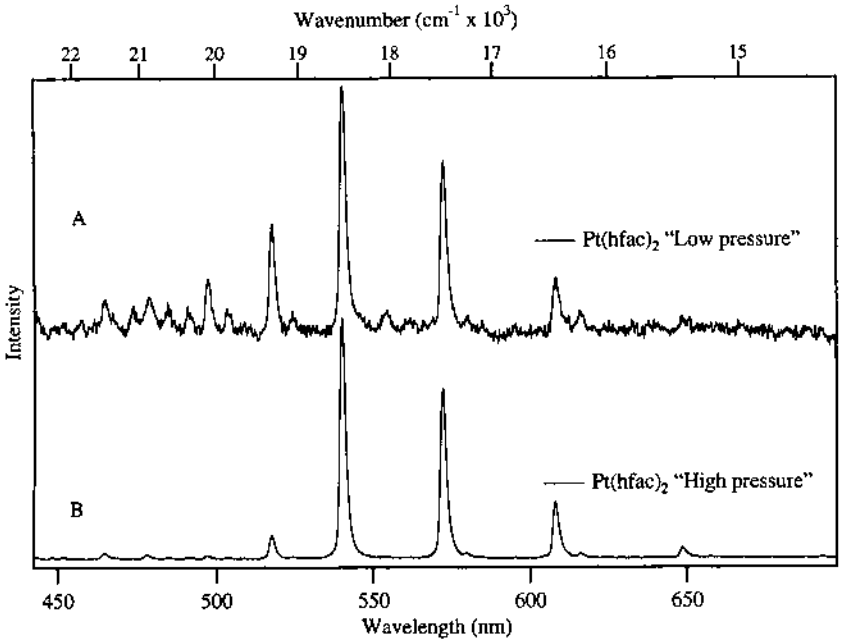

Fig. 3. Emission spectra observed from 440 nm excitation of $Pt(hfac)_2$. (A) spectrum observed at a pressure of no greater than the vapor pressure of $Pt(hfac)_2$ (B) spectrum observed using a static chamber with $Pt(hfac)_2$ at its vapor pressure with ~ 1 bar Ar buffer.

2.5. Mechanisms of fragmentation for metal hfac compounds

2.5.1. Formation of MF and MC

The emission of the diatomic metal fluorides CuF, NiF, and CrF occurs under the collision free conditions of the molecular beam. This observation implies that the formation of this photoproduct is most likely a unimolecular process.

The production of metal monofluorides requires that a large amount of internal motion occur in the molecule such that the fluorine may come in contact with the metal. Intramolecular fluorine atom abstraction by the metal might occur by either or both of two simple mechanisms. The first mechanism involves metal migration as illustrated in the bottom pathway in Fig. 4. Alternate binding modes of metals to β–diketonates are known [23–25], particularly for platinum [23,24], including binding through the pi system (η^3) or binding in a sigma manner (η^1) to the beta carbon. If the metal migrates onto the π system or is bound through the beta carbon, it is much closer to the fluorines on the CF_3 groups than it would be in the standard bidentate binding mode. This mechanism is discussed in more detail in the following section.

A second mechanism which seems more likely for Cu, Ni, and Cr is illustrated in the top pathway in Fig. 4. The single photon absorption at 308 nm has been assigned as a $\pi \rightarrow \pi^*$ ligand centered transition [26,27]. One photon excites the $\pi \rightarrow \pi^*$ system on the ligand and another photon excites a LMCT breaking a M–O bond. The resulting half free ligand is bound through one oxygen. The unbound side can then rotate about the (now) formally C–C single bond placing the CF_3 group in direct contact with the metal. The metal abstracts the fluorine and the resulting MF chemiluminesces. This mechanism involves the least motion of the atoms in the molecule. If a collision occurs before the abstraction takes place, free copper can be produced. However this collision is not required for production of luminescent Ni or Cr.

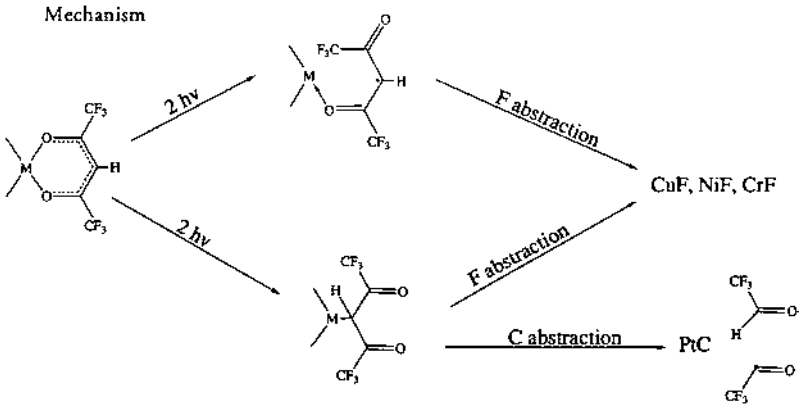

Fig. 4. Proposed intramolecular rearrangements that explain the observed photofragmentation patterns of the metal-hfac compounds studied.

The production of luminescent metal atoms may arise directly from the $M(hfac)_n$ fragmentation process, or it may be a result of absorption of the excitation laser light by either atoms in nonluminescent states or by MF which then fragments to produce $M^* + F$. One note in that regard is that laser induced fluorescence excitation spectra of $Cr(hfac)_3$ show atomic line resonances at 373.08 and 373.20 nm from ground state Cr [28]. This result indicates that Cr atoms are being produced in the ground state upon multi photon fragmentation of the $Cr(hfac)_3$ molecule.

An intriguing and unexpected result of these studies is that of the platinum carbide production. The observed emission spectrum is in excellent agreement with the known $A \rightarrow X$ emission of PtC, and the spectrum was calculated by using literature values [29] for diatomic molecular parameters. Boltzmann fits to the vibrational populations from the luminescence studies were carried out to determine the vibrational temperature of PtC. The fit shows that the ejected PtC is vibrationally hot with a calculated temperature on the order of 1000 K. The ratio of the A state $v = 0$ population to the $v = 1$ population implies a temperature of 870 K. However, the populations of the $v = 2$, 3, 4, 5 states are much higher than predicted for a Boltzmann population at this temperature. Selective population of the higher levels may occur. The PtC fragment produced from the $Pt(hfac)_2$ photofragmentation is vibrationally hot, as is the case for CuF from $Cu(hfac)_2$. The vibrational 'temperature' is substantially lower than those observed for CuF (~ 1700 K). The amount of energy disposed of in electronic and vibrational excitation of the PtC fragment is approximately 30 000 cm^{-1}.

The alternative η^1 binding mode that is specifically known for β-diketonate complexes of platinum is important in the production of PtC. It is a simple matter to eliminate relatively stable fragments from an already Pt–C bonded species to produce the final PtC diatomic as shown in Fig. 4. It cannot be ruled out that binding through the beta carbon of the acetylacetonyl moiety could be involved in the mechanism for the production of metal fluorides. The different patterns (carbides versus fluorides) observed in different metals could be due to the differences in metal binding strength to the beta carbon. Platinum may bind particularly well to the beta carbon, which would explain why this intermediate has been identified previously. The production of PtC has a large driving force; the bond strength of PtC is 50 830 cm^{-1} (145.3 kcal mol^{-1}) [29]. This strong metal carbon bond may substantially weaken the carbon–carbon bonds which results in the mechanism which produces PtC. However, if the metal-–beta carbon bond is weak, then perhaps fluorine abstraction could dominate.

2.6. Summary of metal hfac compounds

Bare metal atoms and diatomic metal fluorides are common photofragments from metal hfac compounds. The spectroscopic studies of UV photofragmentation of $M(hfac)_n$ under a range of gas phase conditions with no surface interactions imply that MF is formed by intramolecular fluorine abstraction by the metal. The MF molecule is both rotationally and vibrationally hot ($T \sim 1700$ K). Although the

one-photon transition in the $M(hfac)_n$ complexes at 308 nm has been assigned as ligand centered $\pi \rightarrow \pi^*$ there is likely some metal contribution to the orbitals involved in the multiphoton transition. Collisions are required for luminescent metal production from $Cu(hfac)_2$ but not from $Cr(hfac)_3$ or $Ni(hfac)_2$.

The production of PtC as a luminescent photofragment from $Pt(hfac)_2$ implies that the type of coordination of the ligand to the metal is very important in determining the photoproduct observed spectroscopically. $Pt(hfac)_2$ is known to bind to the beta carbon of the ligand, and Pt is the only metal for which metal carbide luminescence during photofragmentation is observed.

The spectra from the Ni and Cr compounds contain many atomic lines in addition to the metal fluoride bands. In the case of $Cu(hfac)_2$ atomic lines were observed in the presence of collisions but copper fluoride was found in the absence of collisions. Collisions are not necessary for atomic metal emission in the cases of $Ni(hfac)_2$ and $Cr(hfac)_3$.

Materials deposited by the laser photochemistry of these complexes would be expected to show impurities. Photochemically derived deposits of metals from $Cu(hfac)_2$, $Cr(hfac)_3$, or $Ni(hfac)_2$ are expected to show fluorine incorporation due to the gas phase component of the deposition process. Similarly the photochemical production of platinum metal from $Pt(hfac)_2$ is expected to show carbon contamination [30] because of the production of PtC in the gas phase portion of the deposition process. In all cases, however, the contributions of surface reactions will also be important.

3. Metal sulfide deposition and luminescence spectroscopic identification of photofragments from metal xanthate and thiocarbamate compounds

Important objectives for laser-assisted CVD are wide band gap semiconductors. Intensive research on the growth of wide-band-gap films has included use of pyrolytic CVD [31,32], pulsed laser ablation [33] and molecular beam epitaxy (MBE) [34]. For example, ZnS and ZnSe are currently used as emitting layers in electroluminescent devices and have potential for blue region light emitting diode and laser optoelectronic applications [35–38]. ZnS has a direct band gap of 3.7 eV. Conventional thermolytic MOCVD of ZnS from dual source precursors (e.g. $ZnMe_2$ and H_2S) frequently suffers from problems such as premature reactions between the precursors and high process temperatures [39], resulting in poor quality in homogeneous films [40]. MBE techniques suffer difficulties with stoichiometry control, particularly with respect to sulfur [41].

In this section, deposition of ZnS and ternary ZnCdS from xanthate and dithiocarbamate complexes are reviewed. Results of LCVD studies, identification of luminescent photofragments and mechanisms of gas phase reactions are discussed.

3.1. Metal sulfide formation from zinc xanthate, bis(o-isopropyldithiocarbonato) zinc(II), $Zn(S_2COCHMe_2)_2$ [5]

3.1.1. Photolytic CVD

The zinc xanthate precursor is sublimed into CVD cell under vacuum ($\sim 10^{-2}$ Torr) and irradiated by 308 nm XeCl excimer laser to provide smooth deposits. The photo-deposited films were characterized by surface analytical techniques. Rutherford Back Scattering (RBS) and X-ray photoelectron Spectroscopy (XPS) analysis showed that the films have almost stoichiometric ZnS composition. Scanning electron microscopy (SEM) revealed that the film consists of small granular particles (~ 1 nm in diameter). The grain sizes are about 10 times smaller than those in the thermally-produced films. In the thermally grown films, much larger grain boundaries are possibly formed because of the higher surface mobility at the higher substrate temperature [37]. These experimental results do not conclusively rule out the possibility of a thermal CVD component caused by laser heating of the substrates. However, the similarity of the deposition process on quartz (which does not strongly absorb laser light) and on a Si wafer suggests that heating alone is not the sole cause of the deposition. Photofragmentation studies discussed below show that the process depends on the absorption of light and that gas phase photochemistry occurs.

3.1.2. Luminescence of photofragments

Luminescence is observed in the path of the laser beam in the cell during the course of the laser-assisted CVD studies. The luminescence spectrum is shown in Fig. 5A and exhibits two main features. These are separated by time resolved gated experiments. Under low pressure conditions three sharp bands appear at 468.0, 472.2 and 481.1 nm due to Zn atomic emission (Fig. 5B). Less intense broader, regularly spaced bands (~ 720 cm^{-1} spacing) from 310 to 570 nm are observable in the gated spectra and are assignable to vibrationally hot S_2 as shown in the top trace of Fig. 5C. The top trace of Fig. 5D shows that the time resolved spectrum in the presence of added argon buffer gas (~ 200 mbar) contains a congested progression from 340 to 500 nm which is also assigned to S_2. The bottom trace of Fig. 5D shows a simulated S_2 emission spectrum which matches well with the observed S_2 luminescence.

3.1.3. Fragmentation leading to the luminescent species

The first step of this fragmentation process is a ligand to metal charge transfer (LMCT), which generates $Zn(S_2COCHMe_2)$ and a xanthate radical (Path A of Fig. 6). Both of these fragments are major species in the electron impact mass spectrum. Analogous photo-activated ligand dissociation processes that involve homolytic cleavage of the M–S bond and formation of free ligand have been reported for metal dithiocarbamate complexes [42,43]. Further photofragmentation of the photointermediate $Zn(S_2\ COCHMe_2)$ produces another xanthate radical and a zinc atom (path B of Fig. 6). The luminescence of the zinc atoms probably occurs because the atoms are produced in excited electronic states. Atomic zinc does not have absorption lines at 308 nm and thus cannot be excited directly by the laser.

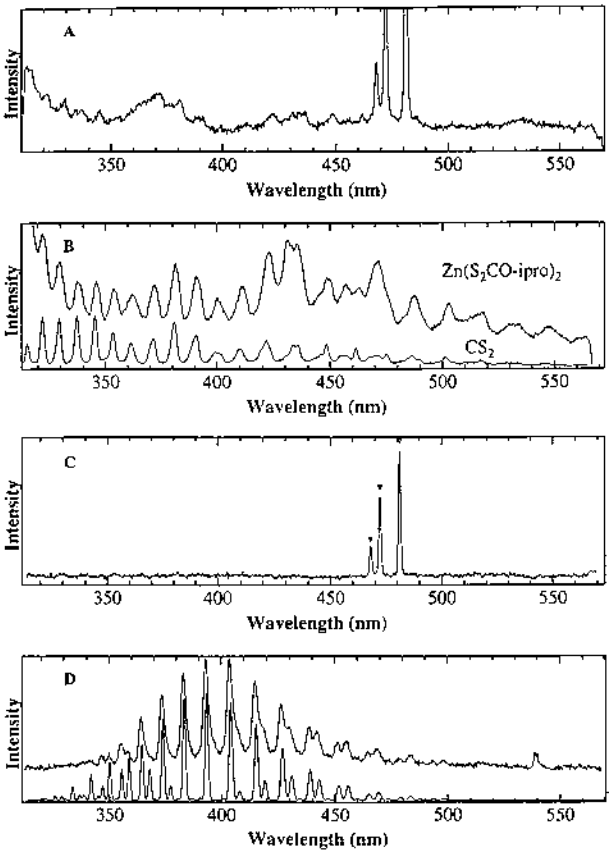

Fig. 5. (A) In situ luminescence spectrum observed during photolytic CVD of $Zn(S_2COCHMe_2)_2$. (B) Gated spectrum observed under low pressure conditions for the 10 ns during the laser pulse. Positions of known Zn atomic emission lines are shown with triangles. (C) The upper trace is the spectrum observed under low pressure conditions delayed 30 ns after the laser pulse and integrated for 40 ns thereafter (hot S_2 emission). The lower trace is the spectrum observed from CS_2 under identical photolytic CVD conditions. (D) The upper trace shows spectrum observed under high pressure conditions delayed 80 ns after the laser pulse and integrated for 10 μs thereafter (collisionally cooled S_2 emission). The lower trace shows a simulated spectrum of the S_2 $B \rightarrow X$ luminescence including contributions from the $n = 0,1,2$ bands in the excited state.

The emission from S_2 arises from further fragmentation steps involving the xanthate radical. The xanthate radical ($^{\bullet}S_2COCHMe_2$) can fragment yielding CS_2 and a isopropyl radical (path C of Fig. 6). Absorption of a UV photon by CS_2 results in fragmentation yielding CS and S. The S atom can further react with CS_2 to produce luminescent S_2 [44]. CS_2 is observed in the laser desorption mass spectra as are S atoms. The low pressure spectrum of zinc xanthate shows features assignable to very hot S_2 ($B \rightarrow X$) [45]. Our photofragmentation control study of CS_2 under identical conditions to those used for the zinc xanthate complex reproduces all of the non-zinc features present in the zinc xanthate photofragmenta-

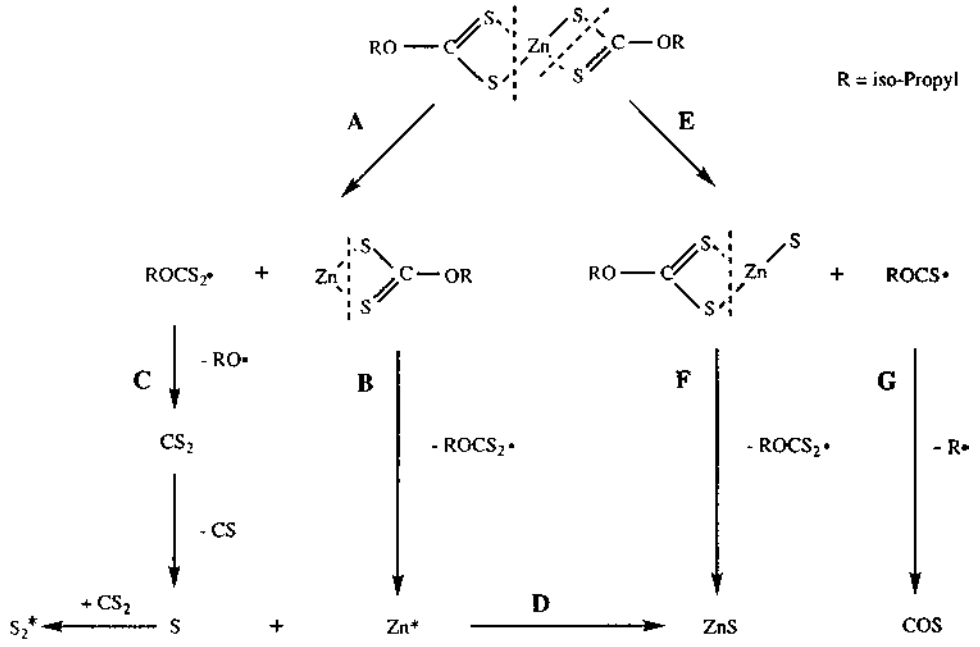

Fig. 6. Photochemically activated fragmentation processes of $Zn(S_2COCHMe_2)_2$ which lead to solid ZnS and to gas phase Zn atom and S_2 luminescence.

tion spectrum which are assigned to S_2 (Fig. 5C). A similar control study of OCS did not give S_2 emission. The spectrum from S_2 observed under higher pressure conditions with added Ar buffer gas shows substantial cooling as a result of collisions (Fig. 5D). Therefore, CS_2 is a photofragment of the zinc xanthate complex. This photoproduct is indicative of complete ligand loss followed by C–O bond cleavage to produce both CS_2 and an isopropoxyl radical (path C). Loss of a second intact ligand (path B) would produce zinc atoms, consistent with the spectra we observe in the gas phase. However, as discussed below, mass spectral evidence shows that loss of the second ligand may not be the exclusive pathway.

3.1.4. Fragmentation leading to ZnS

ZnS is produced by a variety of routes. One of the pathways is implied by the luminescence identification of zinc and sulfur. Combination of these atoms in the gas phase or on the surface leads directly to deposition of the ZnS film (path D of Fig. 6).

A second pathway is illustrated on the right side of Fig. 6. The first step in this process is the loss of ROCS to produce LZnS ($L = S_2COCHMe_2$), i.e. ZnS coordinated by one xanthate ligand (Path E). This species is a major component in the electron impact and laser desorption TOF mass spectra. Photolytic loss of the xanthate ligand from this species, either in the gas phase or on the surface, produces ZnS (path F).

3.1.5. Fragmentation leading to other major species

The electron impact mass data show that the molecular ion $[Zn(S_2COCHMe_2)_2]^+$ is the strongest peak, which implies that the precursor molecule exists as a monomer in the gas phase. Many cracking fragments were identified with the major species being a free xanthate ligand ($S_2COCHMe_2$), a one-ligand complex $Zn(S_2COCHMe_2)$,and a three coordinate complex $Zn(S_2COCHMe_2)S$. Minor species include a three ligand bimetallic complex $[Zn(S_2COCHMe_2)_2 + Zn(S_2COCHMe_2)_1]$, and another three-ligand bimetallic molecule $[Zn(S_2COCHMe_2)_2 + ZnS]$. These results show that the metal ligand (Zn–S) bond and the S–C bond of the ligand are weak. Also, these results suggest that the bonds that are marked by dotted lines in Fig. 6 are relatively weaker than others and that paths A and E are the most important during initial photofragmentation.

The laser desorption mass spectroscopy studies show highly fragmented species from the zinc xanthate compounds. In this process, the precursor was ablated and ionized by N_2 laser irradiation under vacuum ($\sim 10^{-5}$ Torr), with the ionized fragments detected by time of flight mass spectroscopy. The species identified were sulfur, $CHMe_2$, SO, CS_2, ZnS, a xanthate ligand, three coordinate $Zn(S_2COCHMe_2)S$ and the parent compound $Zn(S_2COCHMe)_2$. The presence of the ligand and a three coordinate species support the feasibility of processes A and E in Fig. 6, which is consistent with the electron ionization mass data. The major fragments such as sulfur, propane, CS_2, ZnS are the expected products of the various pathways in Fig. 6.

The organic by-products collected in a liquid nitrogen trap during the photo-CVD process are RH, ROH, CS_2, OCS, R-S-R, and RSH ($R = –CHMe_2$). The presence of RH and ROH supports paths C and G. Direct C–OR dissociation from the parent molecule may also occur. Similarly, CS_2 and OCS are the by-products of paths C and G. The reactive $ROCS^{\bullet}$ radical easily dissociates to give stable species such as OCS and RH, the latter of which is formed by $R^{\bullet}$ abstracting a hydrogen from its surrounding (Path G). It is believed that the other alkyl containing sulfur species (RSH, and R–S–R) were formed via reactive radicals such as $R^{\bullet}$ and $S^{\bullet}$ [46].

All of the species identified by mass spectroscopic data and by trapping the organic byproducts during the photolytic CVD process are consistent with metal-ligand dissociation, C–S bond and C–OR bond cleavage. The reactions shown in Fig. 6 lead to the various organic species identified as well as to inorganic ZnS.

3.2. Multicomponent metal sulfide from metal thiocarbamate compounds [6]

Zn and Cd compounds with the sulfur chelating ligand $S_2CNEt_2^-$ were studied for laser driven materials synthesis. Photodeposition was initiated by using 308 nm light from a XeCl excimer laser. The precursor is sublimed into a CVD cell with a quartz window. The ZnS thin films consist of granules (diameter $\sim 0.2\mu m$) that exhibit a columnar growth pattern by scanning electron microscopic (SEM) analysis. X-ray diffraction (XRD) analyses reveal that the films are highly *c*-axis oriented (002), Wurtzite phase materials [47]. Rutherford back scattering (RBS) analysis

established that the entire film has the stoichiometric composition ZnS. The CdS thin film has a smoother surface without well-defined grain boundaries by SEM analysis. XRD indicates that the films are Wurtzite phase polycrystalline CdS [47]. Both XPS and RBS analyses indicate that the films are pure stoichiometric CdS.

Ternary phase $Zn_xCd_{1-x}S$ thin film were prepared with compositions determined by the amount of each precursor delivered to the CVD chamber. By using this method, any intermediate composition is possible. The Cd and Zn compositions can be estimated from band gap (*Eg*) calculations. The band gaps of the binary (ZnS, CdS) and ternary ($Zn_xCd_{1-x}S$) materials were calculated from optical absorption measurements of the films deposited on quartz substrates [48]. The band gaps for CdS and ZnS were 2.42 and 3.53 eV, in good agreement with the bulk properties of CdS and ZnS (2.43 and 3.66 eV, respectively). The ternary phase materials show bands gaps of 3.29 eV for Zn rich films and 2.53 eV for Cd rich films. The band gap of the ternary phase is known to vary in a quadratic manner with composition; the band gap of 2.53 eV approximately corresponds to a stoichiometry of $Zn_{0.2}Cd_{0.8}S$ and the band gap of 3.29 eV corresponds to $Zn_{0.85}Cd_{0.15}S$ [49].

Luminescence is observed in the path of 308 nm laser beam. This luminescence provides a method of identifying excited photochemical products and intermediates that are formed during the photo-induced CVD process [50]. Under CVD conditions, emissions due to Cd atomic lines were observed at 509 and 480 nm from the cadmium dithiocarbamate precursor (top trace of Fig. 7A) [51]. Less intense regularly spaced bands (~ 720 cm^{-1} spacing) from 330 to 550 nm are also detected and assigned as vibrationally hot S_2 ($B \rightarrow X$) [45]. Very similarly, emission due to Zn atomic lines (472 and 481 nm) and regularly spaced bands (~ 720 cm^{-1} spacing) due to vibrationally hot S_2 ($B \rightarrow X$) were observed from the zinc dithiocarbamate precursor (top trace of Fig. 7B). The production of metal atoms in the gas phase requires multiple ligand dissociations. The emission from S_2 in the gas phase arises from fragmentation steps involving the free dithiocarbamate ligand radical ($^{\bullet}S_2CNEt_2$). Analogous solution phase UV photoactivated ligand dissociation and the generation of the free ligand radical from the metal dithiocarbamate compounds have been reported [42,43]. The radical can fragment yielding CS_2 and NEt_2 radical. Absorption of a UV photon by CS_2 results in fragmentation yielding CS and S. The S atom can further react with CS_2 to produce luminescent S_2 [44]. A photofragmentation control study of CS_2 under identical CVD conditions reproduced all of the non-metal features present in the metal dithiocarbamate photofragmentation spectra which are assigned to S_2 (bottom traces of Fig. 7A,B). The top trace of Fig. 7C shows that the spectrum from the cadmium dithiocarbamate precursor under higher pressure conditions with Ar buffer gas (~ 100 Torr) contains a congested progression from 340 to 500 nm with substantial cooling of S_2 as a result of collisions. The bottom trace of Fig. 7C shows a calculated S_2 ($B \rightarrow X$) luminescence including contributions from $v = 0$, 1, 2 in the excited state.

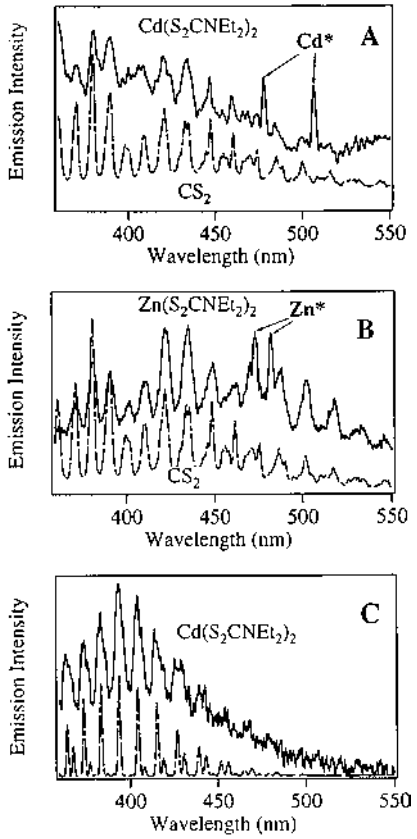

Fig. 7. (A) In situ luminescence spectrum recorded during photolytic CVD from $Cd(S_2CNEt_2)_2$. The top trace is the spectrum observed under low pressure CVD conditions. The bottom trace is the spectrum observed from photolysis of CS_2 under identical conditions. (B) In situ luminescence spectrum observed during photolytic CVD from $Zn(S_2CNEt_2)_2$. The top trace is the spectrum recorded under low pressure CVD conditions. The bottom trace is the spectrum observed from photolysis of CS_2 under identical conditions. (C) The top trace shows a luminescence spectrum observed from $Cd(S_2CNEt_2)_2$ under high pressure conditions (collisionally cooled S_2 emission).The bottom trace shows a calculated spectrum of the $S_2B \rightarrow X$ luminescence.

3.3. Summary of metal sulfide chemistry

Ternary $Z_{nx}Cd_{1-x}S$ films as well as ZnS and CdS films can be prepared photochemically under mild conditions and only in the area irradiated by the laser beam. Luminescence spectra show that the elements composing the films are produced in the gas phase. The results indicate that the deposition process depends on the absorption of light and involves a photochemical component in addition to possible surface adsorption of a photo-intermediate followed by further thermal/photocatalyzed processes on the substrate surface.

4. Metal nitride deposition and luminescence spectroscopic identification of photofragments from metal amide compounds [8]

The metal nitrides are of current interest for microelectronics; TiN in particular is used as a diffusion barrier material in the metalization structures of microelectronic devices [52]. An additional motivation for studying single source precursors for metal nitride formation is the absence of simple sources of nitride ion. Unlike metal sulfides and selenides, for example, where the desired metal cation can react with the chalcogenide anion, metal nitride preparations must employ different strategies such as the one utilized in this work. Both pyrolysis and photolysis of gaseous $Ti(NEt_2)_4$ in the presence of ammonia has been shown to deposit clean TiN [53–61]. The transamination reactions that occur during the thermal CVD involving ammonia have been well studied and are necessary to produce stoichiometric TiN; pyrolysis of the metal amide in the absence of ammonia results in films where the carbon content is usually greater than that of nitrogen. Laser-assisted CVD of $Ti(NEt_2)_4$ in the presence of ammonia also produced stoichiometric TiN; under irradiation the electrical resistivity of the films was lowered [60,61].

4.1. Nanostructrued TiN deposition from $Ti(NEt_2)_4$

Solid thin films of TiN were formed by irradiating $Ti(NEt_2)_4$ gas at 355 nm. The CVD precursor (~ 0.1 g) was heated to its boiling temperature (~ 110–$130°$) in a reservoir cell under vacuum (10^{-2} Torr) and introduced into a CVD cell with quartz windows by using He as the carrier gas. Other gases (e.g. NH_3) were introduced if desired via a different dosing line. The photo depositions were carried out by irradiating a 0.5 cm diameter circle on substrates with ~ 50 mJ/pulse at 20 Hz. Deposits were formed on both quartz and Si (100). The TiN thin films are rough on the surface and consist of granules as shown by transmission electron microscopic analysis. The TEM image shows 11 ± 3 nm diameter granules of TiN on the quartz substrate. Auger Electron Spectroscopy and EDS comparison with a TiN standard indicate that the films are stoichiometric TiN within the experimental uncertainty; a small amount of oxygen contamination is detected while almost no carbon is present, similar to the results reported for 193 nm irradiation [60,61].

4.2. In situ spectroscopic studies of MN formation in the gas phase

Spectroscopic investigations of the photofragmentation reactions that lead to the deposition were carried out under two gas phase conditions: a gas cell at about 10^{-1} Torr, and the collision-free conditions of a supersonic expansion molecular beam (10^{-6} Torr). The former reproduces the conditions used for the deposition of films and includes molecular collisions (but not collisions with surfaces) while the latter restricts the photochemistry to intramolecular reactions.

Luminescence was observed when each of the metal amide complexes was irradiated at 308 nm in a 6-way cross gas cell under conditions similar to those used for the deposition studies. The luminescence spectra from the fragmentation of

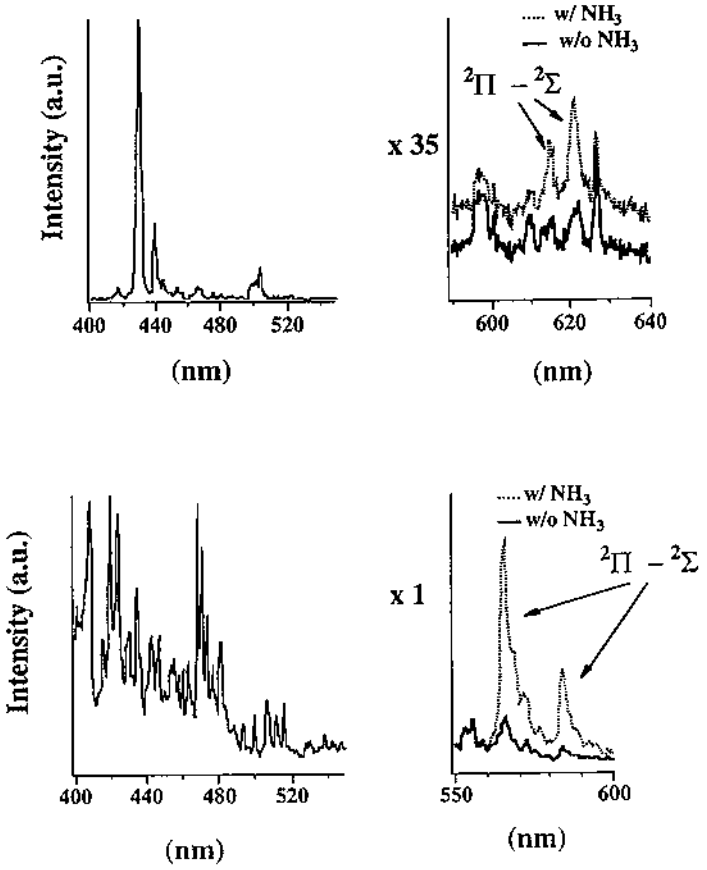

Fig. 8. Emission spectra during photolysis of $Ti(NEt_2)_4$(top) and $Zr(NEt_2)_4$ (bottom) in the gas phase. Two spectral regions are shown. The 400–550 nm region is dominated by the emission of the metal atom. The bands at 613.9 and 619.9 nm in the spectrum from $Ti(NEt_2)_4$ and the bands at 564.2 and 587.9 nm in the spectrum from $Zr(NEt_2)_4$ are the $^2\Pi \rightarrow {}^2\Sigma$ emissions from diatomic TiN and ZrN, respectively. The intensities of these bands increase in the presence of ammonia gas (dotted lines).

$Ti(NEt_2)_4$ and $Zr(NEt_2)_4$ are shown in Fig. 8. The region between 400 and 500 nm in each spectrum is dominated by the emission of the metal atoms. These atomic lines are well known and the assignment is unambiguous [62,63]. In addition to the atomic lines, well known emission bands from CH (431.4, 432.4 nm) and C_2 (468.4, 469.8, 471.5, 473.7 nm) are observed [45]. Similar assignments are made for the emission spectrum obtained when the Hf complex is photolyzed. The identification of bare Ti, Zr or Hf atoms and diatomic ligand fragments shows that extensive fragmentation takes place.

The most important luminescence are the bands at 613.9 and 619.9 nm in the spectrum of $Ti(NEt_2)_4$ and the bands at 564.2 and 587.9 nm in the spectrum from $Zr(NEt_2)_4$ (Fig. 8). In both cases, the emission bands have been assigned to the

$A^2\Pi_{3/2} \rightarrow X^2\Sigma^+$ and $A^2\Pi_{1/2} \rightarrow X^2\Sigma^+$ transitions, respectively, in diatomic MN [64–66]. (Because emission from HfN has not been reported in the literature, it is not known if any of the unassigned bands in the spectrum involving $Hf(NEt_2)_4$ arise from HfN.) The spectra in Fig. 8 unambiguously show that TiN and ZrN are produced in the purely gas phase component of the deposition process. Furthermore, these diatomics are not the result of reactions with a source of nitrogen other than the amide ligand; only the precursor molecules and He buffer gas are present in the cell.

The addition of ammonia gas resulted in a dramatic increase in the intensity of the TiN and ZrN emission (Fig. 8, inset). Ammonia increased both the rate of film deposition and the purity of the film. Similar trends during pyrolytic CVD were attributed to ammonia coordination followed by enhanced elimination of NR_2H [57–59]. The luminescence studies show that ammonia is not necessary for gas phase MN formation, but that it enhances MN formation.

To test whether or not the MN formation was intramolecular or whether it required intermolecular reactions, the photofragmentation was studied in the collision free environment of a molecular beam. In order to identify MN as well as of other photofragments, time of flight mass spectroscopy was used. Mass spectroscopy confirmed the formation of the bare metal and the ligand fragments observed in the emission spectra. Large peaks from the amide ligand and partially dissociated metal complexes (the heaviest being $Hf(NEt_2)_3$ were also observed. Most importantly, mass selection provided unambiguous identification of the HfN diatomic.

4.3. Summary of MN chemistry

Diatomic metal nitrides are produced in the gas phase under laser-assisted CVD conditions. The amide ligand can act as the source of the nitride, and the photoreaction produces the metal nitride via an intramolecular process in the absence of collisions. When collisions are frequent, MN is also produced when the only reactants are the precursor molecules, but the production of MN is enhanced in the presence of ammonia gas. Characterization of the TiN photodeposit shows that 11 ± 3 nm crystalline nanoparticles of TiN are formed. These results suggest that interesting nucleation pathways are followed that may enable nanocrystals to be collected, and that photolysis is a convenient method of making solid metal nitrides.

5. Summary

Spectroscopic identification of fragments of precursor coordination compounds for laser assisted CVD that are produced in the gas phase provides information about the photochemical reaction pathways. Studies of metal compounds with three different ligand systems (diketonate, thiocarbamate, and amide) that serve as precursors for various materials such as metals and semiconductors were reported.

The luminescence of gas phase neutral intermediates directly identify desired (e.g. TiN) and undesired (e.g. CuF) species that affect the composition of the deposit. The observation of gas phase fragments under the actual deposition conditions during the materials synthesis is important not only to monitor the growth process but also to elucidate the mechanistic aspects of photofragmentations of the coordination compounds. This review provides a glimpse of the complex deposition processes that can be observed spectroscopically. The field is in its infancy; a combination of luminescence spectroscopy (that can be used to identify neutral and charged luminescent species) and mass spectroscopy (that can be used to identify ions) will continue to assist in understanding and developing LCVD protocols and will continue to provide surprises about the gas phase photochemical products.

Acknowledgements

J.I.Z. thanks the US National Science Foundation (CHE-9816552) and J.W.C. thanks KOSEF (1999-1-122-001-5) for supporting this work.

References

[1] For reviews, see (a) J.G. Eden, Photochemical Vapor Deposition, Wiley, New York, 1992 (b) M.L. Hitchman, K.F. Jensen, Chemical Vapor Deposition: Principles and Applications, Academic Press, San Diego, 1993 (c) T.T. Kodas, M.J. Hampden-Smith, The Chemistry of Metal CVD, Weinheim, New York, 1994 (d) J. Chaiken (ed.), Laser Chemistry of Organometallics, ACS Symp. Ser, 1993, p. 530.
[2] (a) K.L. Kompa, Angew. Chem. Int. Ed. Engl. 27 (1988) 1314. (b) I.P. Herman, Chem. Rev. 89 (1989) 1323. (c) J.G. Eden, Photochemical Vapor Deposition, Wiley, New York, 1992.
[3] (a) J. Sykora, J. Sima, Coord. Chem. Rev. 107 (1990) 1. (b) G.L. Geoffroy, M.S. Wrighton, Organometallic Photochemistry, Academic Press, New York, 1979.
[4] D. Wexler, J.I. Zink, L.W. Tutt, S.R. Lunt, J. Phys. Chem. 97 (1993) 13563.
[5] J. Cheon, D.S. Talaga, J.I. Zink, J. Am. Chem. Soc. 119 (1997) 163.
[6] J. Cheon, J.I. Zink, J. Am. Chem. Soc. 119 (1997) 3838.
[7] J. Cheon, D.S. Talaga, J.I. Zink, Chem. Mater. 9 (1997) 1208.
[8] J. Cheon, M. Guile, P. Muraoka, J.I. Zink, Inorg. Chem. 38 (1999) 2238.
[9] D.S. Talaga, J.I. Zink, Inorg. Chem. 35 (1996) 5050.
[10] D.S. Talaga, S.D. Hanna, J.I. Zink, Inorg. Chem. 37 (1998) 2880.
[11] M.L. Hitchman, K.F. Jensen, Chemical Vapor Deposition: Principles and Applications, Academic Press, San Diego, 1993.
[12] T.T. Kodas, M.J. Hampden-Smith, The Chemistry of Metal CVD, Weinheim, New York, 1994.
[13] H.D. Kaesz, R.S. Williams, R.F. Hicks, J.I. Zink, Y.J. Chen, H.J. Muller, Z.L. Xue, D.Q. Xu, D.K. Shuh, Y.K. Kim, New J. Chem. 14 (1990) 527.
[14] P. Doppelt, T.H. Baum, MRS Bull. 19 (1994) 41.
[15] D.L. Schulz, T.J. Marks, Adv. Mater. 6 (1994) 719.
[16] M. Nemoto, M. Yamanaka, J. Mater. Res. 5 (1990) 1.
[17] C.R. Jones, F.A. Houle, C.A. Kovac, T.H. Baum, Appl. Phys. Lett. 46 (1985) 97.
[18] F.A. Houle, R.J. Wilson, T.H. Baum, J. Vac. Sci. Technol. A 4 (1986) 2452.
[19] J.S. Cohan, H. Yuan, R.S. Williams, J.I. Zink, Appl. Phys. Lett. 60 (1992) 1402.
[20] E.B. Flint, J. Messelhauser, H. Suhr, Appl. Phys. A 53 (1991) 430.

[21] P.B. Kargl, R. Kullmer, D. Bauerle, Appl. Phys. A 57 (1993) 175.
[22] A.A. Avey, R.H. Hill, J. Am. Chem. Soc. 118 (1996) 237.
[23] G.T. Behnke, K. Nakamoto, Inorg. Chem. 6 (1967) 440.
[24] F.D. Lewis, A.M. Miller, G.D. Salvi, Inorg. Chem. 34 (1995) 3173.
[25] S. Kimiya, J.K. Kochi, J. Am. Chem. Soc. 99 (1977) 11.
[26] D. Wexler, J.I. Zink, Inorg. Chem. 35 (1996) 4064.
[27] J.P. Fackler, F.A. Cotton, D.W. Barnum, Inorg. Chem. 2 (1963) 97.
[28] D.S. Talaga, PhD thesis, University of California, Los Angeles.
[29] Données Spectroscopiques relatives aux Molécules Diatomiques, 17th ed., B. Rosen, (Ed.), Pergamon Press, New York, 1970, p. 515.
[30] P. Mogyorosi, J.O. Carlsson, M. Moradi, Appl. Surf. Sci. 54 (1992) 46.
[31] J.W. Li, Y.K. Su, M. Yokoyama, Jpn. J. Appl. Phys. 35 (1996) 5050.
[32] P.B. Smith, J. Vac. Sci. Technol. A. 7 (1989) 1451.
[33] M. Mclaughlin, H.F. Sakeek, P. Maguire, W.G. Graham, J. Molloy, T. Morrow, S. Laverty, J. Anderson, Appl. Phys. Lett. 63 (1993) 1865.
[34] M. Kitagawa, Y. Tomomura, K. Nakanishi, A. Suzuki, S. Nakajima, J. Cryst. Growth. 101 (1990) 52.
[35] S. Yamaga, Jpn. J. Appl. Phys. 30 (1991) 437.
[36] G.F. Neumark, R.M. Park, J.M. Depuydt, Physics Today June (1994) 26.
[37] M. Ohring, The Materials Science of Thin Films, Academic Press, San Diego, 1992.
[38] I.P. McClean, C.B. Thomas, Semicond. Sci. Technol. 7 (1992) 1394.
[39] H. Kukimoto, J. Cryst. Growth. 107 (1991) 637.
[40] K.P. Giapis, K.F. Jensen, J.E. Potts, S.J. Pachuta, J. Electron. Mater. 19 (1990) 453.
[41] H. Ando, A. Taike, M. Konagai, K. Takahashi, J. Appl. Phys. 62 (1987) 1251.
[42] D.F. Schwendiman, J.I. Zink, J. Am. Chem. Soc. 98 (1976) 4439.
[43] K.W. Given, B.M. Mattson, M.F. McGuiggan, G.L. Miessler, L.H. Pignolet, J. Am. Chem. Soc. 99 (1977) 4855.
[44] S.P. Sapers, N. Andraos, D.J. Donaldson, J. Chem. Phys. 95 (1991) 1738.
[45] R.W.B. Pearse, A.G. Gaydon, The Identification of Molecular Spectra, Chapman and Hall, London, 1976.
[46] Similar explanations have been also reported on radical species of other chalcogene elements. (a) L. Henriksen, in: S. Patai (Ed.), The Chemistry of Organic Selenium and Tellurium Compounds, vol. 2, Wiley, New York, 1987. (b) H.J. Gysling, A.A. Wernberg, T.N. Blanton, Chem. Mater. 4 (1992) 900.
[47] JCPDS Powder Diffraction File, W.F. McClune (Ed.), International Center for Diffraction Data, Swarthmore, PA, 1990.
[48] The optical band gaps of the materials are calculated from a plot of $(\alpha)^2$ (where α is absorption coefficient) versus photon energy ($h\nu$): J.I. Pankove, in Optical Process in Semiconductors, Prentice-Hall, Englewood Cliffs, New Jersey, 1971 (Chapter 1).
[49] The formula $Eg(x) = xEg_{(ZnS)} + (1-x)Eg_{(CdS)} - x(1-x)b$ is used for the calculation, where x is the fractional composition and b is a bowing parameter which represents the non-linearity of the band gap changes (0.61 for $Zn_xCd_{1-x}S$ system).
[50] Gas phase photoluminescence spectra were obtained by passing the emitted light through a 0.3 m Spex HR 320 single monochromator and recording the spectra by using an EG&G OMA III Princeton Applied Research 1421 optical multichannel analyzer.
[51] Wavelength and Transition Probabilities for Atoms and Atomic Ions, US Department of Commerce, National Bureau of Standards, US Government Printing Office, Washington DC, 1980, NSRDS-NBS 68.
[52] K. Littau, G. Dixit, R.H. Havemann, Semiconductor International July (1994) 183.
[53] R.M. Fix, R.G. Gordon, D.M. Hoffman, J. Am. Chem. Soc. 112 (1990) 7833.
[54] R.M. Fix, R.G. Gordon, D.M. Hoffman, Chem. Mater. 3 (1991) 1138.
[55] D.M. Hoffman, Polyhedron 13 (1994) 1169.
[56] T.R. Cundari, J.M. Morse, Chem. Mater. 8 (1996) 189.
[57] B.H. Weiller, J. Am. Chem. Soc. 118 (1996) 4975.

[58] J.A. Prybyla, C.-M. Chiang, L.H. Dubois, J. Electrochem. Soc. 140 (1993) 2695.
[59] L.H. DuBois, Polyhedron 13 (1994) 1329.
[60] U. Illmann, R. Ebert, G. Reisse, H. Freller, P. Lorenz, Thin Solid Films 241 (1994) 71.
[61] S. Ishihara, M. Hanabusa, J. Appl. Phys. 84 (1998) 596.
[62] W.L. Wiese, G.A. Martin, Wavelength and Transition Probabilities for Atoms and Atomic Ions, US Gov. Printing Office, Washington, 1980.
[63] A.R. Striganov, N.S. Sventitskii, Tables of Spectral Lines of Neutral and Ionized Atoms, IFI/Plenum, New York, 1968.
[64] T.M. Dunn, L.K. Hanson, K.A. Rubinson, Can. J. Phys. 48 (1970) 1657.
[65] J.K. Bates, T.M. Dunn, Can. J. Phys. 54 (1976) 1216.
[66] C.M.-T. Chan, H. Li, S-K. Sze, A.S.-C. Cheung, J. Mol. Spectrosc. 180 (1996) 145.